I. J. Engineering and Manufacturing, **2022, 5, 22-47**
Published Online on October 8, 2022 by MECS Press (http://www.mecs-press.org/)
DOI: 10.5815/ijem.2022.05.03

Dynamic Modelling and Control of Flapping Wing Micro Air Vehicle for Flap-Glide Flight Mode

Lidiya Abebe Dejene
Addis Ababa Science and Technology University/College of Electrical and mechanical Engineering/Department of Electromechanical Engineering, Addis Ababa, Ethiopia
Email: lidabebe92@gmail.com

Received: 07 April 2022; Revised: 18 May 2022; Accepted: 13 June 2022; Published: 08 October 2022

Abstract: Flapping wing micro-air-vehicles (FWMAV) are micro-air-vehicles that use biomimetic actuation (oscillatory flapping wing) for aerodynamic force generation. The realization of such bionic flight, which offers small size, low speed, and flexible maneuverability has significant military and civilian values. Thus the design of FWMAV (ESB-I) will be very important for security related sectors since they have all the right stuffs for surveillance and reconnaissance. Since everything about a bird is made for flight the kinematic and dynamic modeling as well as control algorithm of bird like FWMAVs is more complex than that of serial robots. Thus balancing the main requirements for the design of FWMAVs which includes excellent aerodynamic performance, high efficiency, and satisfactory maneuverability is very important. With the aim to improve the performance of a FWMAV this work incorporates an intermittent flapping and gliding flight mode. Flap-gliding flight mode, which is often used by large bird species, effectively combines the aerodynamic advantages of fixed and flapping wings. Inspired from it, a kind of flexible flap-gliding Micro Air Vehicle, named Ethio-Smart Bird-I (ESB-I), was successfully designed. An expression describing the mechanical energy cost of travelling of this flight mode in terms of work per range for one flap-glide flight cycle was presented. It is shown that there is an energy saving of flap-gliding flight compared to continuous flapping flight. However due to a system dynamic variation in this flight mode, it possesses difficulty in control surface design. To implement this specific flight mode, this thesis proposes a closed-loop active disturbance rejection control, ADRC, strategy to stabilize the attitude during the processes of flapping flight, transition and gliding flight. To verify the control effect, the unsteady aerodynamic estimation method of the flapping wing based on modified strip theory approach and the dynamics of the FWMAV in Lagrangian form were modelled in the MATLAB/SIMULINK platform and applied in the simulation. Using this model longitudinal stability of ESB-I was analyzed. Simulation results show that even if the FWMAV is in different flight modes, ADRC controller can track the target pitch signal effectively with tracking error less than 0.05rad. To further explain the effects of ADRC in this specific flight mode, the control effects of a PID controller is presented. As per the simulation result ESB-I with PID controller has a target pitch angle tracking error greater than 1rad. This shows that, in flap-gliding flight mode ADRC can track the target pitch signal better than PID controller.

Index Terms: Flapping wing micro-air-Vehicle, Flap-glide flight, Active Disturbance Rejection Controller.

1. Introduction

One of the oldest dreams of mankind is to fly like a bird, to move freely through the air in all dimensions. Thus For thousands of years human beings have been exploring the flight mechanism of natural flying organisms to realize bionic flight. From Leonardo Da Vinci's drawings to Otto Lilienthal's gliders, the first five hundred years of flapping flight research focused on human transport. However, despite the invention of aircraft which has fixed and rotary wings and its wide application, bionic flight with low energy and high mobility similar to flying organisms has not been successful.

In order to develop a new type of platform different from fixed- and rotary-wing aircraft, for decades, Roboticists and biologists have studied the appearance, movement, and behavior of natural flying organisms which generate the required aerodynamic forces by flapping their wings. Such agile flight has significant military and civilian value. The emphasis on this type of flight necessitates the realization of bionic flight, which offers small size, low speed, and flexible maneuverability at low speeds. Inspired from birds FWMAV can be designed to adopt various single flight modes like flapping, gliding, hovering, or multi flight modes.

The proposed FWMAV, ESB-I, adopts intermittent flapping and gliding flight which effectively combine aerodynamic advantages of fixed and flapping wings. This strategy also will give the wing movements a more natural sight, and this is essential when realizing applications of any FWMAV in surveillance.

Since everything about a bird is made for flight the kinematic and dynamic modeling as well as control algorithm of bird like FWMAVs is more complex than that of serial robots. Thus balancing the main requirements for the design of FWMAVs which includes excellent aerodynamic performance, high efficiency, and satisfactory maneuverability is difficult. Moreover the characteristics of the aerodynamic forces exhibit large variations in flap-glide flight mode, which adds challenges to the control surface. Therefore there is a need for more effort when designing a FWMAV which adapts a flap-gliding flight mode to guarantee the FWMAV is airborne.

In the proposed work a problem related to longitudinal attitude control of FWMAVs that adapts multiple flight mode, in this case flap-glide flight mode, will be addressed.

In the proposed work, the author first shows the benefits of flap-gliding flight mode by comparing ESB-I in flap-glide flight mode with continuous flapping flight mode. And then address a problem related to longitudinal attitude control of FWMAVs that adapts multiple flight mode, in this case flap-glide flight mode. Thus main objective of the proposed work is to conceptually design a reference FWMAV, ESB-I, which adapts flap-gliding flight mode through a consecutive computational tasks to obtain aerodynamic and geometric parameters of the wing and sizing the flapping mechanism, and design dynamic model and controller to guarantee the longitudinal stability of the vehicle.

2. Litrature Review

For steady, level flight in still air, modern airplanes are particularly effective. Propellers produce efficient thrust, and today's cambered airfoils are extremely. Examining performance in more fascinating flying regimes, on the other hand, explains why birds and insects remain the true acrobats of the sky. Despite the fact that insect flight has been a fascinating subject for at least half a century, significant attempts to duplicate it are relatively new. This area received a major boost in 1996, when the Defense Advanced Research Projects Agency of the United States (DARPA) launched a three-year MAV to develop a surveillance and reconnaissance flying platform with a length of less than 15 centimeters. Since then, a great deal of effort has gone into developing FWMAVs. Fig. 1 depicts some recent examples of typical FWMAVs.

Fig. 1(a) shows a MAV with 16.5cm wingspan and 19g mass named “Nano Humming Bird” which was designed by AeroVironment in 2011. It uses an actuation mechanism composed of rollers and strings for the two flapping wings. The vehicle adapts hovering flight mode only and could hover for 11 min with approximately 30 Hz of flapping frequency and forward speed up to 6.7 m/s.

Fig. 1(b) and Fig. 1(c) shows the two FWMAVs “SmartBird” inspired by herring gull and “BionicOpter” inspired by dragonfly which were launched by Festo in 2011 and 2013 respectively. These FWMAVs have 200cm and 63cm wingspan with 450 g and 175 g mass respectively. The Smartbird uses a planar eight-bar flapping wing mechanism to flap its two foldable flapping wings. Whereas the BionicOpter uses its four individually adjustable wings which could almost move in any orientation in space for demonstrating its hovering performance. It is clear that in both of these FWMAVs a flapping wing mechanism that leads to an increase in complexity of a control system and vehicle weight was used to adapt just a single flight mode.

The Chinese “Dove” shown in Fig. 1 (d) was also one of the recent successful FWMAV launched by Northwestern Polytechnical University (NPU) from 2012-2017. It has a mas of 220 g with wingspan of 50cm. It uses a planar 4 bar single crank double rocker actuating mechanism for flapping its two wings. Such mechanism creates unsymmetrical motion between the two wings. Similar to the previous ones Chinese Dove also adapt single flight mode for its cruise for flight which is flapping mode.

When looking at their control mechanism since the above discussed and other previously MAVs adapt a single flight mode, most of them applies a conventional controller applicable for the specific flight mode to stabilize the attitude of the vehicle. If the flight mode considered was a low-frequency flapping flight mode most of the previous works uses the proportional-integral derivative (PID) control technique. Such closed-loop attitude control system gives the FWMAV the ability to fly towards a target. Whereas if the flight mode considered was a gliding flight mode since such flight mode is almost the same with the flight pattern of fixed-wing aircraft the common closed loop vehicle attitude control technique applied for a fixed-wing aircraft can be applied. Thus most previously designed FWMAV which adapt a gliding flight mode a uses a controller, such as adaptive control methods and robust control methods with only slight changes.

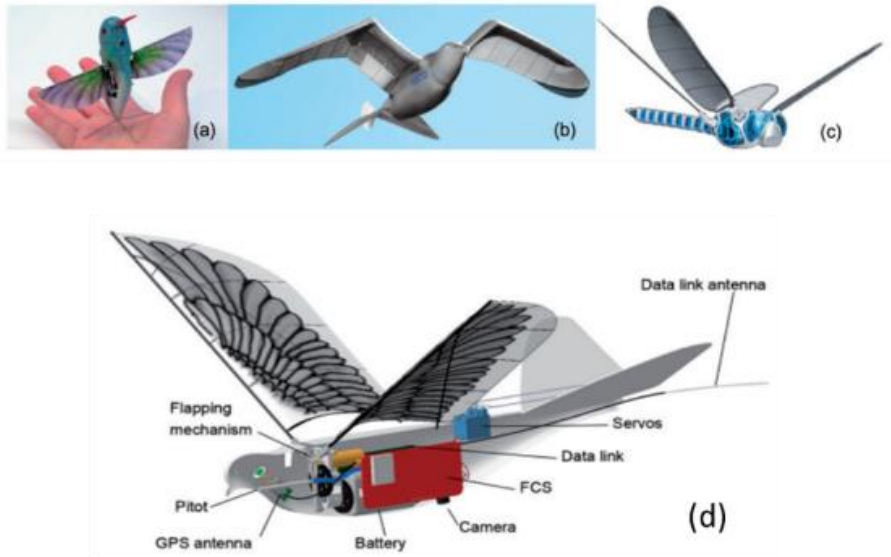

Fig. 1. Typical FWMAVs: (a) Nano Humming Bird, (b) Smart Bird, (c) BionicOpter, and (d) Chinese Dove [2]

The main objective of the proposed work is to conceptually design a reference FWMAV, ESB-I, which adapts flap-gliding flight mode and design dynamic model and controller to guarantee the longitudinal stability of the vehicle. ESB-I uses a simple light weight planar 4 bar single crank double rocker flapping wing mechanism as in the Chinese Dove but with a modification that makes the mechanism Symmetric which make the design process easier.

Also unlike most of the works done previously, ESB-I will adopts flap-gliding flight which has a potential to reduce energy consumption in return increase efficiency. This strategy also make the wings movement more natural thus applicable for surveillance and reconnaissance applications. Thus while designing controller for ESB-I this flight mode will be considered.

In flap-gliding flight mode the properties of the aerodynamic forces change dramatically during the shift from the flapping mode to the gliding mode and vice versa. Thus if one apply a conventional control technique for attitude control of the vehicle, such as PID, for this specific flight mode, the control surface's efficiency steadily declines owing to system dynamic fluctuation. As a result, the traditional control technology, such as the PID controller, loses its control effect, potentially resulting in a flight mishap.

Thus to ensure stable closed loop longitudinal attitude control during each modes , flapping and gliding as well as the transition process between them, the proposed work will present an active disturbance rejection control (ADRC) technique to address the problems encountered in flap-gliding flight mode.

Generally, compared with above discussed and other previous works, the main contributions of the proposed work are as follows.

1. The reference FWMAV model (ESB-I) adapt flap-glide flight mode
2. Conceptual design and dynamic modeling ESB-I conducted assuming ESB-I adapt flap-gliding flight mode. In addition to increasing biomimetic level, this strategy also has the potential to reduce energy consumption compared to continuous flapping flight.
3. An ADRC strategy will be applied to control the attitude of ESB-I during flap-gliding flight mode.

3. Methodology

The design process for MAV can be seen as very similar to other aerial vehicles. However, since MAVs are very small in size the complexity in the design process increased. More over effect of their flapping wing makes the design process very much complex compared to fixed wing large aerial vehicles like conventional airplane.

Here the reference FWMAV, ESB-I, will adopt intermittent flap-gliding flight mode. To make the design process easier similar to successfully launched previous FWMAVs the overall layout of ESB-I will be classified in to three main subsystems: (1) Flapping wing mechanism subsystem; (2) Flight control and navigation subsystem and (3) Mission Payload subsystem. The flapping wing mechanism subsystem is primarily concerned with the design of a flapping wing mechanism that converts electrical energy from the onboard battery into mechanical flapping power for the wings, with efficiency and robustness being the most important considerations. The flight control and navigation subsystem is responsible for attitude control and navigation of ESB-I. The last subsystem, Mission Payload has a task related to the specific application of the vehicle, such as surveillance. However as already stated the focus of this thesis is in the first two subsystem functions, i.e. Conceptual design of the flapping wing subsystem and attitude control of the designed system for stable flight. The general process flow chart is shown in Fig. 2 below.

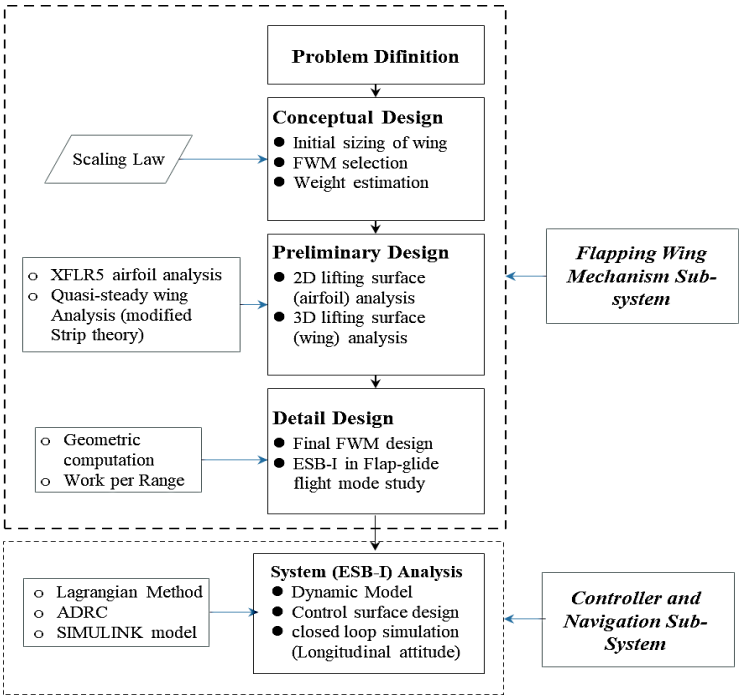

Fig. 2. The reference model, ESB-I's design process and system dynamics and controler design flowchart

As shown in Fig. 2 above, in the proposed methodology the whole task is divided into 4 parts. In conceptual design stage considering the specific flight mode, flap-glide, through a consecutive computational tasks initial aerodynamic and geometric parameters of the wing were obtained and sizing the flapping mechanism accomplished. In preliminary stage 2D lifting surface analysis to choose the best airfoil for ESB-I and 3D lifting surface analysis to obtain aerodynamic model for ESB-I takes place. Then using the obtained model in the remaining parts aerodynamic advantages of F-flap-glide flight mode over continuous flight mode were investigated. Finally dynamic modeling and designing ADRC for ESB-I was accomplished and longitudinal attitude stability of ESB-I presented. These parts will be presented in the consecutive sections.

3.1 Conceptual Stage

In this section conceptual design of ESB-I is presented.

3.1.1 Initial Sizing of wing

In the conceptual design phase of wing sizing, a scale law was used, which was a biological statistics in mathematical language compiled by Shyy et al. [3]. According to this law using geometric similarity approach one can get approximate values for the geometric and aerodynamic design parameters such as wing span, wing area, wing loading, aspect ratio, and wing beat frequency.

Table 1. Scaling of wing parameters

Quantity	**Relationship**	**Result**
Wingspan, b(m)	Fixed	0.7
Mass, M(kg)	$m = 0.85b^{2.56}$	$0.265 \cong 0.3$
Wing Area, S(m^2)	$S = 0.16M^{0.72}$	$0.0672 \cong 0.07$
Aspect Ratio, AR	$AR = b^2/S$	$\cong 7$
Wind Loading, W/S (N/m^2)	$W/S = 62.2M^{0.28}$	$\cong 44.4$
Flapping Frequency, f(Hz)	$f = 3.87M^{-0.27}$	$5.76 \cong 6$

In addition to Aspect Ratio Taper ratio (λ) is one of important parameter to decide on the planform of the wing. According to [4] as cited in [5] it was deduced that the inner part of the wing contributed mostly to lift creation, whereas the outer part of the wing was the primary source of thrust, with deformations predominating. As a result, a robust flapping-wing design should have enough lifting surface in the inner part and a flexible trailing edge area in the outer part to generate significant thrust, and the planform should be roughly a trapezium to meet a preferred taper ratio. However, the wing tip area has a significant impact on power consumption, thus the wing tip area should be limited. A chamfer angle on the trailing edge would be an acceptable solution to achieve these requirements. Thus for easy of

aerodynamic analysis two generic wing planforms were chosen considering the above empirical study; semi-elliptical planform and approximate quarter circle planform and are shown in Fig. 3.

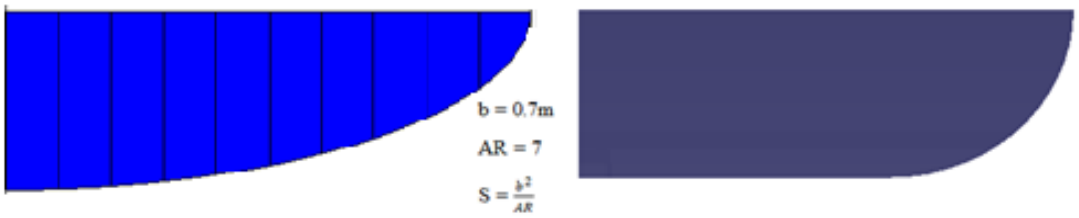

Fig. 3. Generic wing planforms semi-elliptical (first), quarter circle (second)

3.1.2 Flapping Wing Mechanism selection

To transform the electrical energy from the battery into a flapping motion, FWMAV uses a wide range of actuation methods. Four-bar mechanisms are commonly employed in mechanism design, and a flapping motion can be achieved depending on their arrangement and relative size. When choosing these mechanisms, many important criteria must be evaluated and compared in order to choose the best actuator for the FWMAV design.

In the proposed system, hybrid actuation mechanism which is presented by Hassanalian et al. [6] will be used. The qualities of an alternating crank mechanism and a slider-crank mechanism are combined in this actuation device. These two actuation mechanisms work together to provide a lightweight system that maintains harmonic flapping frequencies between the two wings. The selected hybrid flapping wing mechanism is shown in Fig. 4.

Fig. 4. Schematic view of hybrid mechanism with flapping motion only [6].

3.2 Preliminary Design

Engineers take one step further in the design process to build a basic proof of concept in the preliminary design phase. The engineers will compute the requirements that the MAV must meet in order to fly.

3.2.1 2D Lifting Surface Analysis

The procedure of determining the airfoil section for a wing is covered in this section. It is proper to say that after wing planform, the airfoil section is the second most essential wing parameter. Airfoil design and airfoil selection are the two methods for determining the wing airfoil section. Because designing an airfoil is a time-consuming and complex procedure, in this thesis an airfoil among the currently existing airfoils based on the mission requirements will be selected.

For selecting airfoil for ESB-I a methodology proposed by Taimur et al. [8] is used. To apply the above airfoil selection procedure first one need to select a list of airfoils which best suited for low Reynold number ($10^4 - 10^5$) flight. For this purpose 10 air foils were chosen from a website [9] and their performance parameters were generated using XFLR5 software. Then parameter τ_{air} (related to airfoil efficiency) and η_{air} (related to airfoil performance) will be calculated. Here a MATLB program is developed which takes the airfoil parameters as an input argument and calculates τ_{air} and η_{air} for each airfoils. Finally it chooses the best airfoil by comparing their τ_{air} and η_{air}. If τ_{air} and η_{air} values conflict an average of them Σ_{air} will be calculated and it will decide the output. Based on this procedure S1091 airfoil was chosen. Fig. 5 and Fig. 6 shows the selected air foil view and its detail xflr5's analysis output respectively.

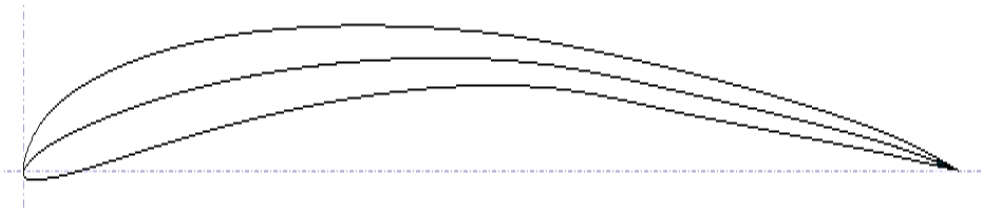

Fig. 5. S1090 airfoil. Thickness = 5.06%, maximum thickness position at 13.42%, Maximum camber = 6.06% and maximum camber position at 45.15% of chord length.

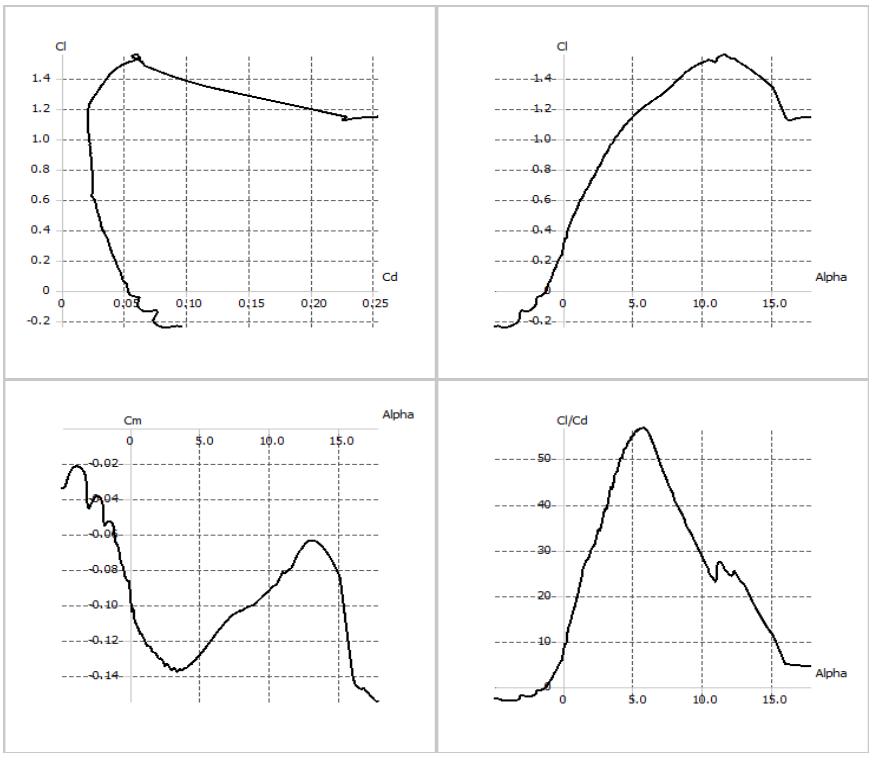

Fig. 6. XFOIL analysis result for S1091 airfoil. (a) Variation of lift coefficient with drag coefficient; (b) Variation of lift coefficient with angle of attack, from this graph $\alpha_0 = -1.25,\ \alpha_{stall} = 11.6,\ C_{l,max} = 1.561$; (c) Variation of pitching moment coefficient with angle of attack, this graph can be used to get C_{m0}; (d) Variation of ratio of lift to drag coefficient with angle of attack, this graph gives $\left(\frac{C_l}{C_d}\right)_{max}$

3.2.2 3D Lifting Surface Analysis

Here procedures for this analysis basically follows pitching-flapping motion of the generic wing planform and most of this procedure are adopted from the work of DeLaurier [10], Harmon [11], and Malik et al [2]. To show the effect of different aerodynamic parameters on aerodynamic forces parametric study will be carried out.

3.2.2.1 3d Wing Aerodynamic Modeling

Blade element theory is one of the methodologies that has been used to explore flapping wing aerodynamics. The analytical modeling for aerodynamic forces and moments will be done using Blade Element Analysis (quasi steady approach) since it is a basic analytical technique that can produce appropriate findings without the complexity of computational methods.

The following assumptions were made for the following aerodynamic models: The wings are formed of a flexible membrane with a spar at the leading edge; only flapping with identical up/down flapping angles would be induced by the power train system; Both flapping and pitching motions are assumed to be sinusoidal functions with a certain amount of lag.

As already stated the designed flapping wing will have two distinct motions with respect to two axes which are Flapping and passive pitching. The flapping angle φ and pitching angle ϑ vary as a cosine function, as given by (1).

$$\begin{gathered}\varphi(t)=\varphi_0 Cos(\omega t)\\ \delta\vartheta=(\vartheta_0 r)Cos(\omega t+\Phi)\\ \vartheta(t)=\delta\vartheta+\bar{\vartheta}\end{gathered} \tag{1}$$

Where: φ_0 and ϑ_0 are flapping angle amplitude and Dynamic twist in deg/m respectively, Φ is lag angle between pitching and flapping and r is span wise distance along the wing. The lag between pitching and flapping angle should be such that the pitch angle is maximal when the relative air velocity is highest. It is possible only if the lag is 90^0. $\bar{\vartheta}$ is the sections mean pitch angle and it is the sum of the flapping axis angle with respect to flight velocity (incidence angle, $\bar{\vartheta}_a$), and the mean angle of the chord line with respect to the flapping axis, $\bar{\vartheta}_w$. i.e. $\bar{\vartheta} = \bar{\vartheta}_a + \bar{\vartheta}_w$. This angle, $\bar{\vartheta}$, is defined to accommodate for the possibility that the chord's mean pitch angle with respect to the flapping axis is not zero.

When the leading edge is used as a reference point, the wing's motion is broken down into three distinct motions: plunging, pitching, and forward motion relative to the freestream velocity (U). The velocity distributions operating on the wing during downstroke are depicted in Fig. 7.

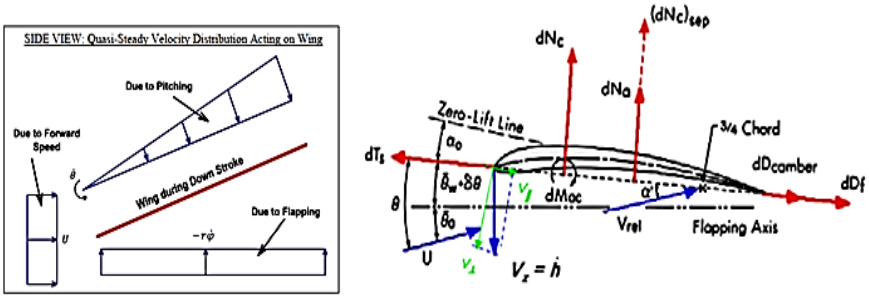

Fig. 7. Quasi-steady velocity distribution acting on the flapping wing. (a) Assuming γ and $\bar{\vartheta}_a$ zero, (b) detail illustration; based on [10]

Fig. 7(b) illustrates the component of plunging velocity $\dot{h}$ in a direction perpendicular to the airfoil chord line seen at each instant of time is $\dot{h}cos(\bar{\vartheta} - \bar{\vartheta}_a)$. In pitching motion, the ¾ chord point is the point of concern, and then the radius of rotation ¾ chord giving a rotational velocity equals $\frac{3}{4}c\dot{\vartheta}$. Finally in forward motion, the instantaneous relative angle of attach $\delta\vartheta$ giving a velocity in vertical direction $U\delta\vartheta$ $(U(\vartheta - \bar{\vartheta}))$. The relative AOA which results from wing motion discussed above, at ¾ chord location can easily be calculated as:

$$\alpha = \frac{\left(\dot{h}Cos(\vartheta - \bar{\vartheta}_a) + \frac{3}{4}c\dot{\vartheta} + U(\vartheta - \bar{\vartheta})\right)}{U} \tag{2}$$

As already indicate blade Element Analysis is used to perform the aerodynamic analysis. In this method, a time-dependent problem is turned into a series of separate, steady-state problems, and the forces are calculated using steady-state aerodynamics. Because of unstable wake-effects, the net aerodynamic forces are reduced due to the limiting wing span. Theodorsen function [2] can be used to account for these impacts.

Fig. 7 (b) shows wing's section aerodynamic forces and motion variables. No linear variation of the wing's dynamic twist will be assumed without losing generality (i.e. $\bar{\vartheta}_w = 0$), so that $\bar{\vartheta}$, mean pitch angle of chord with respect to flapping axis, can be simply assumed to be equal to the incidence angle, $\bar{\vartheta}_a$ throughout the present work. i.e. $\bar{\vartheta} = \bar{\vartheta}_a$

The vertical and horizontal components of the wing's resultant force are known as lift, thrust, and drag. The aerodynamic model used in this thesis includes effects of camber, downwash effect, leading edge suction, and post-stall behavior to obtain these forces. The strip theory approach assumes that the aspect ratio of the wing is large enough to allow the flow over each section to be treated as essentially chordwise (in the free-stream direction

The section's total attached flow normal force acting perpendicularly to the chord line and acting along and parallel to the chord line will be given by:

$$\begin{cases} dN = dN_c + dN_{nc} \\ dF_x = dT_s - dD_{camber} - dD_f \end{cases} \tag{3}$$

Now the resulting sectional instantaneous Lift and Thrust forces at each strip dr, respectively can be given by:

$$\begin{cases} dL = dNCos\vartheta + dF_x Sin\vartheta \\ dT = dF_x Cos\vartheta - dNSin\vartheta \end{cases} \tag{4}$$

Also the total sectional drag can be expressed as:

$$dD_{total} = dNSin\vartheta + (dD_f + dD_{camber})cos\vartheta \tag{5}$$

To obtain a three dimensional instantaneous lift and thrust for each wing, these expressions should be integrated along the span; hence

$$L(t)=2\int_0^{b/2} Cos(\varphi(t))dL$$
$$T(t)=2\int_0^{b/2} dT \tag{6}$$

In (6), $\varphi(t)$ is the section's dihedral angle at that instant in the flapping cycle.

The wings average lift and thrust are obtained by integrating L(t) and T(t) over the cycle. To do this, it was found most convenient to perform the integration with respect to cycle angle, s, instead of time, t, where: $s = \omega t$. Thus the average lift and thrust for one cycle can be given by:

$$\bar{L}=\frac{1}{2\pi}\int_0^{2\pi} L(s)ds$$
$$\bar{T}=\frac{1}{2\pi}\int_0^{2\pi} T(s)ds \tag{7}$$

The total moment, dM generated by the flapping wing is sum of section's pitching moment about its aerodynamic center which depends on the airfoil characteristics, dM_{ac} and dM_a which includes apparent-camber and apparent-inertia moments, and given by [10]:

$$dM=dM_{ac}+dM_a$$
$$dM_{ac}= C_{mac}\frac{\rho}{2}U^2Sc$$
$$dM_a= -\left(\frac{1}{16}\rho\pi c^3\dot{\vartheta}U+\frac{1}{128}\rho\pi c^4\ddot{\vartheta}U\right) \tag{8}$$

Where C_{mac} the co-efficient of moment about aerodynamic center, S is the wing surface area. Then the average aerodynamic moment can be given by:

$$\bar{M} = \frac{1}{2\pi}\int_0^{2\pi}\left(2\int_0^{b/2} dM(s)\right)ds \tag{9}$$

Now average aerodynamic forces and moments for the two wing planforms chosen in conceptual design stage can be obtained. The analysis is based on values from Table 1: wingspan 0.7m, aspect ratio 7, flapping frequency 6Hz, total flapping angle 60 º, forward speed 7m/s, dynamic twist 10 º, and incidence angle 6 º and lag angle of 90 º. The results from the two wing planforms are shown in Fig. 8

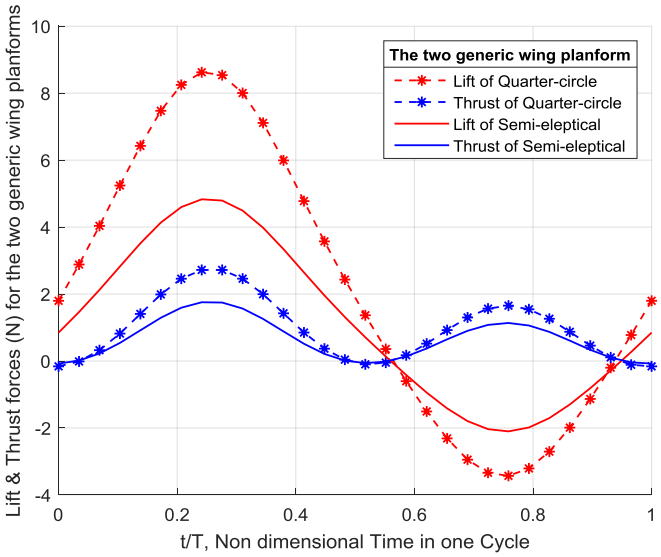

Fig. 8. Comparition between aerodynamic force outputres of the two generic wing planforms.

From Fig. 8 one can see that the quarter-circle wing planform gives average lift and thrust of 2.2 and 0.97 respectively for the given parameters shown. This shows that the lifting and thrusting capacity of the wing increased significantly with the generic approximate quarter wing planform compared to the generic semi-elliptical wing planform. Even though there is a significant increase in lift with the selected wing planform, still there should be some modification to achieve the required load carrying capacity of the wing. So in the next section effects of various aerodynamic parameters on lift, thrust and drag will be studied.

3.2.2.2 Parametric Study

In this section the effects of important aerodynamic parameters on lift, thrust and drag will be studied. These parameters are: flapping frequency, f, forward speed, U, incidence angle, ϑ_a, total flapping angle, $2\varphi_0$, and dynamic twist ϑ_0. The parametric study results are shown from Fig. 9 to Fig. 13.

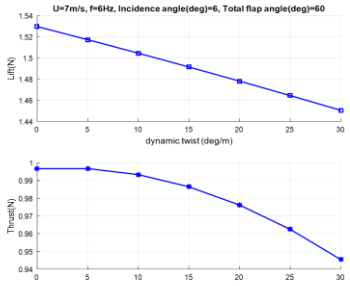

Fig. 9. Variation in Lift and Thrust with dynamic twist (ϑ_0)

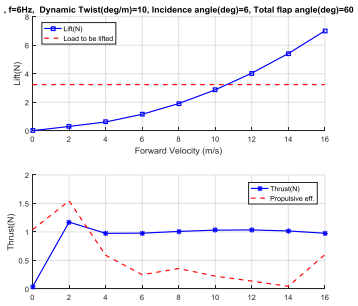

Fig. 10. Variation in Lift and Thrust with forward velocity (U)

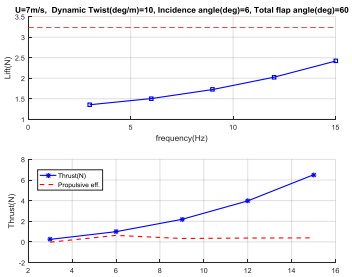

Fig. 11.Variation in Lift, Thrust and Drag with flapping frequency

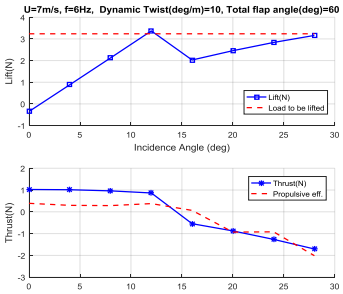

Fig. 12. Variation in Lift and Thrust with incidence angle (ϑ_a)

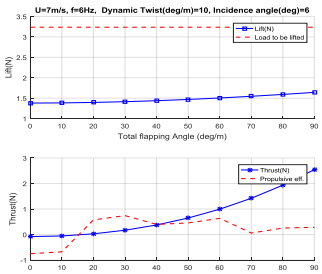

Fig. 13. Variation in Lift and Thrust with total flapping angle ($2\varphi_{max}$)

Generally:

a) Forward speed have the greatest impact on ESB-I's lift, while flapping frequency has the least impact.
b) Thrust of ESB-I is most affected by flapping frequency and incidence angle but least affected by forward speed.
c) Dynamic twist has least effect on both lift and thrust

Now based on the parametric study a computation is performed to find all the optimal combinations of dynamic twist (ϑ_0), total flapping angle ($2\varphi_0$), incidence angel ($\bar{\vartheta}_a$), flapping frequency (f) and optimal forward flight speed (U) for optimal flight of ESB-I. The manual optimization is based on the following requirements:

a) Average Lift condition: The main requirement is that the average Lift for a flapping cycle must be greater than or equal to the weight W≈3.1N, i.e.(L≥W).
b) Average propulsive efficiency condition: The average propulsive efficiency should be in the limit: $0 < \eta_{prop} < 1$.. The propulsive efficiency can be formulated using DeLaurier model [10] as: $\eta_{prop} = \frac{TU}{P_{in}}$.

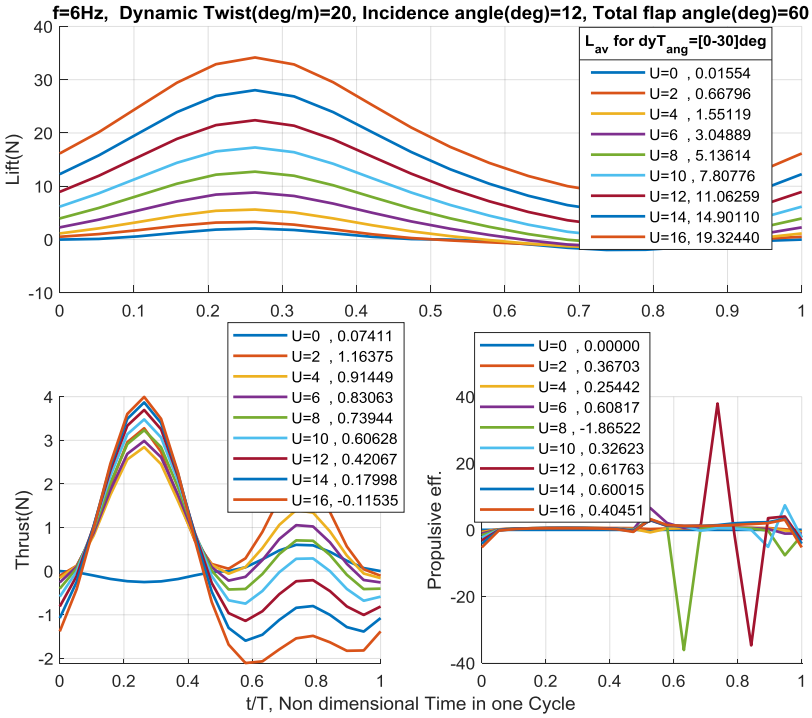

Fig. 14. Lift, Thrust and propulsive efficiency for last choosen aerodynamic parameters from manual itteration

As indicated in Fig. 14, based on the above requirement, the aerodynamic parameters chosen for optimal performance of ESB-I are: $\vartheta_0 = 20deg/m$, equal upstroke and down stroke amplitude of $\varphi_0 = 30deg$, $\bar{\vartheta}_a = 12deg$, $f = 6Hz$ and $U = [7 - 12]m/s$.

3.3 Detail Design

3.3.1 Final sizing of the Flapping mechanism

In the selected mechanism the connector member with the help of the guidance bars will act as a slider-crank mechanism that generates vertical reciprocating motion.. The connecting rod then translates the connector member's reciprocating action into an oscillating motion in the rocker. A two dimensional schematic view of the mechanism is shown in Fig. 15 below.

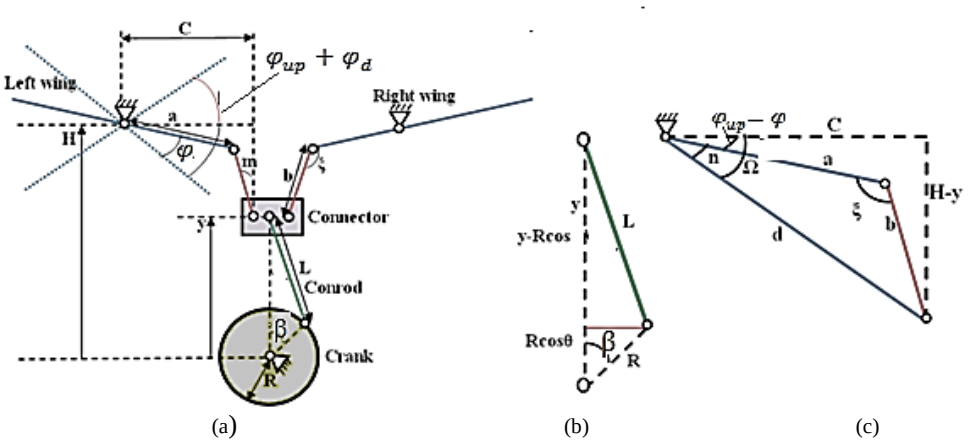

(a) (b) (c)

Fig. 15. (a) 2D view of the flapping mechanism, (b) crank, Conrod, and connector member, and (**c**) a triangles from mechanism components.

Where: R: Radius of crank, L: length of Conrod, b: length of the connecting rode, a: length of the rocker, β: Crank angle, φ: Flapping angle, and ξ: Transmission angle

Taking length parameters as design variables some of the design constraints that should be considered are:-

1. *Total range of wing angle* (i.e. total flapping angle = 2φ) – the upstroke (φ_{up}) and downstroke angles (φ_d), here considered equal, and are two known parameters based on the preliminary stage wing sizing.
2. *Minimizing ratio of L/R* – The connecting member's motion should be harmonic to avoid severe influences on the mechanism. The L/R ratio should be increased for a well-defined value of the crank's radius R in order to make connector member motion harmonic. On the other hand, in order to avoid increasing the mechanism's total weight, this parameter should be carefully chosen.
3. *Minimizing transmission angle (ξ)* - The transmission angle of the mechanism should fulfill the minimum transmission requirement to ensure good transmission performance.

3.3.1.1 Determining the Minimum Ratio of L/R

As shown in Fig. 15(b), considering the crank, Conrod and connector member as a slider crank mechanism, one can get the equations of position (y), velocity ($\dot{y}$), and acceleration ($\ddot{y}$) for the connector member as follow:-

$$L^2 - R^2 sin^2\beta = (y - Rcos\beta)^2$$
$$y = R\left(\sqrt{(L/R)^2 - sin^2\beta} + cos\beta\right) \quad (10)$$

$$\dot{y} = -R\omega\left(\frac{sin2\beta}{2\sqrt{(L/R)^2 - sin^2\beta}} + sin\beta\right) \quad (11)$$

$$\ddot{y} = -R\omega\left(\frac{cos2\beta}{\sqrt{(L/R)^2 - sin^2\beta}} + \frac{sin^2 2\beta}{4((L/R)^2 - sin^2\beta)^{3/2}} + \cos\beta\right) \quad (12)$$

In (11) and (12) angular velocity of crank, $\omega = \dot{\beta}$ can be related with the flapping frequency as ω = 2πf. To get the minimum approximate value of L/R that makes the motion of the connector member harmonic, first let's plot a graph that shows the non-dimensional position, velocity and acceleration of the connector member vs crank angle. Then the minimum value of L/R that makes the curve closer to harmonic will be chosen as optimum value.

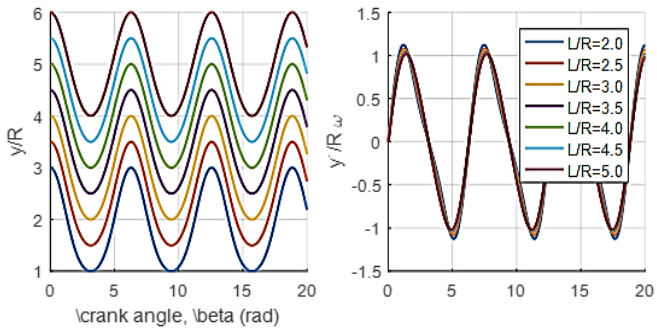

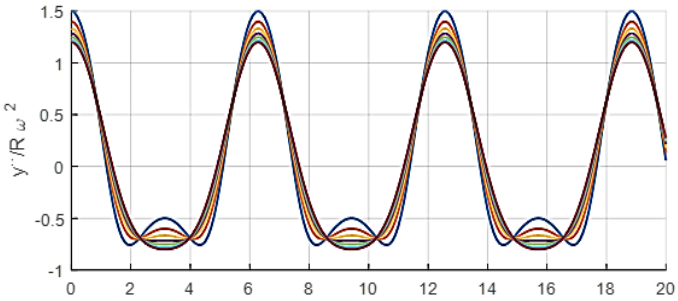

Fig. 16. Variations in the connector member's non-dimensional acceleration as a function of crank angle for various L/R ratios when the flapping frequency is set to 6Hz.

As shown in Fig. 16 below, when L/R is greater than 3.5, this curve approaches the harmonic shape. When the variations of dimensionless acceleration as a function of crank angle are investigated, it is discovered that L/R = 4 is the smallest allowable value in order to obtain harmonic oscillations.

3.3.1.2 Determine dimensions of the actuation mechanism

In this section the relationships between the flapping angle (φ), the crank angular position (β), and other parameters that influence the flapping angle will be determined. From Fig. 15 the transmission angle (ξ) can be expressed as:

$$\xi = cos^{-1}\left(\frac{d^2-a^2-b^2}{-2ab}\right)$$

$$\xi = cos^{-1}\left(\frac{C^2+\left(H-R\left(\sqrt{(L/R)^2-sin^2\beta}+cos\beta\right)\right)^2-a^2-b^2}{-2ab}\right) \tag{13}$$

Again from Fig. 15(c) a relation is obtained as follow:

$$(\varphi_{up}-\varphi) = \Omega - n = \ tan^{-1}\left(\frac{H-y}{C}\right) - sin^{-1}\left(\frac{bsin\xi}{d}\right) \tag{14}$$

Hence the flapping angle can be given by:

$$\varphi = \varphi_{up} - (\Omega - n)$$

$$\varphi = \ \varphi_{up} - \left(tan^{-1}\left(\frac{H-y}{C}\right) - sin^{-1}\left(\frac{bsin\xi}{d}\right)\right) \tag{15}$$

Where $d = \sqrt{C^2 + (H-y)^2}$

Then inserting equations of y, d and ξ in (15), one can get the detail expression for the flapping angle. Finally by differentiating, one can get expressions of the angular velocity and acceleration of the rocker (i.e. flapping angular velocity and acceleration of ESB-Is wings).

$$\dot{\varphi} = \omega\left(\frac{R\left(\frac{sin2\beta}{2\sqrt{(L/R)^2-sin^2\beta}}+sin\beta\right)}{\frac{a(C-\text{acos}(\varphi_{up}-\varphi))-\text{sin}(\varphi_{up}-\varphi)}{b\sqrt{1-\left(\frac{C-\text{acos}(\varphi_{up}-\varphi)}{b}\right)^2}}-\text{acos}(\varphi_{up}-\varphi)}\right) \tag{16}$$

Inspecting (13) and (16) the effective parameters affecting the flapping, φ, and transmission, ξ, angles are common, those parameters are a, b, H, C R, and L/R. Thus, these two angles should be determined simultaneously.

Based on preliminary stage results and above discussed constraints, 5 modes were obtained through successive improvement stages. Finally mode-5 which satisfies all of the required conditions were chosen. Fig. 17 show the variations of the flapping angle (φ) and the transmission angle (ξ) as a function of the crank angle (β) for the last chosen mode. The oscillations of the flapping and transmission angles has harmonic shape.

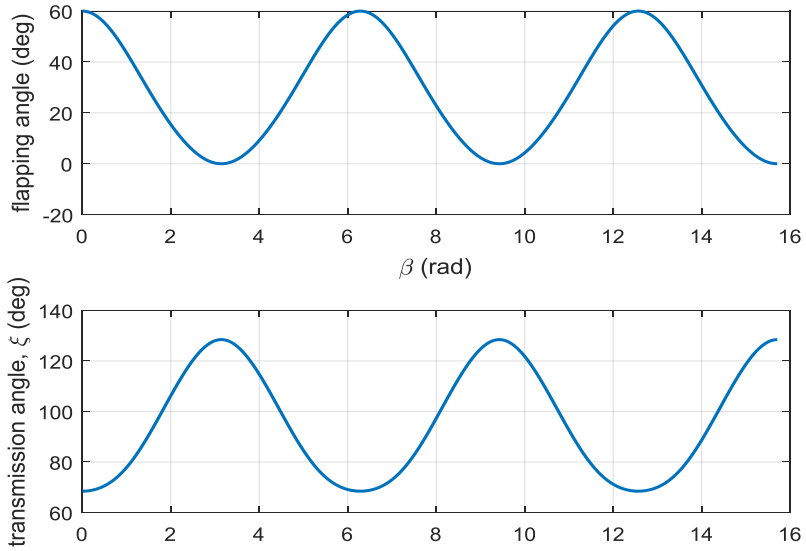

Fig. 17. Variations of flapping angle, φ (top) and transmission angle, ξ (bottom) as a function of the crank angle (β) for the fifth mode.

3.3.1.3 Required Torque and Power

After determining the dimensions of the actuation mechanism, the required torque and power for the crank rotation was determined in order to give the required aerodynamic force for the flapping wing. The relation between the required torque and the aerodynamic force can be given by the equations:

$$\tau_{crank}=\frac{-2\vec{F}_{aero}\overrightarrow{V_F}}{\dot{\beta}} \qquad dP_{in}=-2\vec{F}_{aero}\overrightarrow{V_F} \tag{17}$$

Where: $\vec{V}_F$: Linear velocity of wings due to flapping (which includes velocity components due to plunging, $\dot{h}$ and pitching, $\dot{\vartheta}$), $\dot{\beta}=\omega$ is crank Angular velocity and $\vec{F}_{aero}$ is the aerodynamic force generated due to actuation of the flapping mechanism. From aerodynamic analysis the instantaneous power required to move the section against its aerodynamic load for attached flow is given by:

$$dP_{in}= dF_x\dot{h}\sin(\vartheta-\bar{\vartheta}_a)+dN\left(\dot{h}\cos(\vartheta-\bar{\vartheta}_a)+\frac{1}{4}c\dot{\vartheta}\right)+dN_{nc}\frac{1}{4}c\dot{\vartheta}-dM\dot{\vartheta} \tag{18}$$

The instantaneous crank input power absorbed by the whole wing is then found from the integration all over the span, and the average input power throughout the cycle is obtained by the integration all over the crank rotation cycle, β.

$$\bar{P}=\frac{2}{2\pi}\int_0^{2\pi}\int_0^{b/2}dP_{in}(r,\beta) \tag{19}$$

The variations of angular wing motion due to actuation mechanism using the evaluated dimensions of the mechanism, and required torque as a function of the crank angle, respectively are shown in Fig. 18. The figure also shows the maximum, minimum, and mean values of the required torque for the crank rotation. Then the maximum and mean values of the required mechanical power are obtained as $35.92\ W$ *and* $12.63\ W$ respectively.

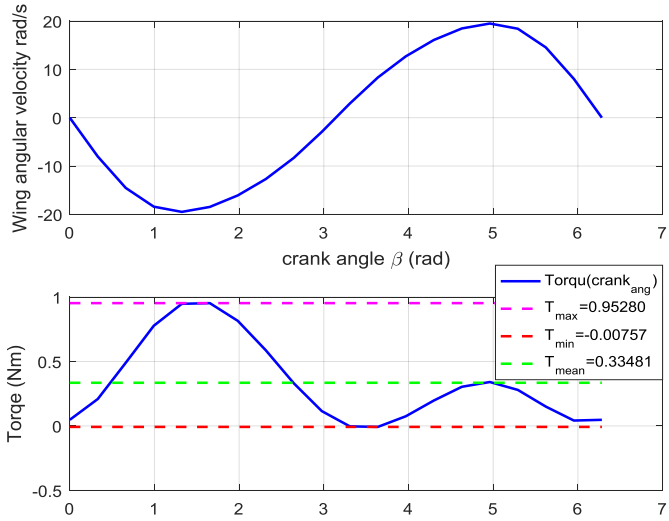

Fig. 18. Variations of wing angular velocity,$\dot{\varphi}$ (top), required torque, τ_{crank} (bottom) as a function of the crank angle, β

3.3.2 Advantage of Flap-glide flight mode

In the next section, advantage of the specific flight mode compared to continuous flapping flight mode will be shown. Flap-glide (Undulating) flight is one mode of intermittent flight which is much more wide-spread among large birds. In this mode a periods of flapping are followed by gliding periods.

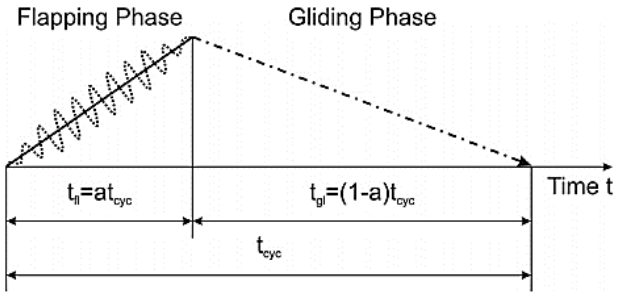

Fig.19. Flap-gliding flight (According to Rayner et al. $\boldsymbol{t_{cyc}}$: total cycle time, ***a:*** flapping ratio

As shown in Fig.19, the basic element of flap-gliding flight is a cycle that comprises of two phases, one of which is active flapping flight and the other is gliding flight. The potential energy state of the bird is enhanced in the flapping phase by ascending (at an angle θ_{cl}) to a greater altitude, whereas in the non-flapping phase, the bird glides (at an angle θ_{gl}) to the altitude at the start of the cycle.

In this section a model for flap-gliding flight of FWMAV's and the accompanying mechanical energy cost of travel is presented. Consider a FWMAV with a flight path angle, θ_{cl}, taking force in x direction the following equation obtained:

$$T - Wsin(\theta_{cl}) - D = \frac{W}{g}\frac{dU_{fl}}{dt} \tag{20}$$

Where W=mg, Rearranging and multiplying both sides of the above equation by U_{fl}, results:

$$(T - D)U_{fl} = W(U_{fl}sin(\theta_{cl}) + \frac{d}{dt}\frac{{U_{fl}}^2}{2g}) \tag{21}$$

Also $U_{fl}sin(\theta_{cl})$ is the sinking speed, V_s of the vehicle, and it can be related to the lost altitude during gliding as, $V_s = \frac{dh}{dt}$. Thus can be rewritten as:

$$(T - D)U_{fl} = W\frac{d}{dt}\left(h + \frac{{U_{fl}}^2}{2g}\right) \tag{22}$$

The left side of (22) represents the rate of change of net mechanical energy or excess power during flapping phase and the right side represents rate of change of kinetic and potential energy of the FWMAV.

In flapping phase the wings shape and motion gives the FWMAV the lift and thrust force required to be air born, however, in gliding phase the FWMAV can support its weight with its wings, but does no mechanical work. Hence, as shown in (22), the excess energy accumulated during the flapping phase can be used to compensate for the drag work performed during the gliding period.

Further considering the FWMAV in constant climb during flapping, (22) reduced to:

$$P_{ex} = (T - D)U_{fl} = W\frac{d}{dt}(h) \tag{23}$$

Thus for being able to conduct a glide such that the energy state at the end of a flapping phase cycle is the same as at the at the end of a gliding phase, it is necessary that the excess power produced during flapping phase should be able to compensate the aerodynamic power required during gliding phase as a potential energy loos.

From Fig.19 the flapping phase has duration $t_{fl} = at_{cyc}$ and the gliding phase has duration $t_{gl} = (1 - a)t_{cyc}$. Then, in the flapping phase, work provided by the mechanical power output is:

$$W_{cyc} = P_{ava}at_{cyc} \tag{24}$$

Then the energy state balance of the entire flap-gliding flight cycle become:

$$(P_{ex})at_{cyc} = P_{aero,gl}(1 - a)t_{cyc} \tag{25}$$

To study the flap-glide flight mode in one cycle, it is necessary to describe the work per range of one flap-glide cycle. The range travelled in a cycle of flap-gliding flight can be expressed as:

$$x_{cyc} = at_{cyc}U_{fl}\cos(\theta_{cl}) + (1 - a)t_{cyc}U_{gl}\cos(\theta_{gl}) \tag{26}$$

Then based on the above equations, the work per range can be expressed as:

$$\frac{W_{cyc}}{x_{cyc}} = \frac{P_{ava}P_{aero,gl}}{P_{aero,gl}U_{fl}\cos(\theta_{cl}) + P_{ex}U_{gl}\cos(\theta_{gl})} \tag{27}$$

Since speeds during flapping and gliding phases, U_{fl} and U_{gl}, are different, the average speed of a flap-gliding flight can be given as:

$$V_{fl-gl} = a\,U_{fl} + (1 - a)\,U_{gl} \tag{28}$$

3.3.2.1 Aerodynamic power in the flapping and gliding phases

During the gliding phase the aerodynamic power due to the drag acting on the FWMAV is given by:

$$P_{aero,gl} = D_g U_{gl} \tag{29}$$

Since during gliding mode the FWMAV is the same as a fixed wing vehicle, aerodynamic modeling approach for fixed wing aircraft can be applied Thus total drag force on the FWMAV can be modeled as the sum of the induced (D_{in}) and parasite (D_{par}) drag in the way that parasite drag includes the two drags of profile and shape. The induced drag is given by [11]:

$$D_{in} = C_{D,in}\frac{\rho}{2}U_{gl}^2 S = \frac{2KL^2}{\pi AR\rho S U_{gl}^2} \tag{30}$$

Where C_L is the lift coefficient, $C_{D,in}$ induced drag coefficients, K is the induced drag factor and can be obtained using Oswald number (e) as $K = \frac{1}{e}$, and AR is aspect ratio. Experimental data suggest that $K \approx 1.1 - 1.2$ [16].

The parasite drag is calculated using the Tucker method. This method begins by using Prandtl equation [11] to calculate the coefficient of frictional drag (C_f) of a flat sheet in turbulence.

$$C_f = 0.455\,(\log_{10} Re)^{-2.58} \tag{31}$$

Where Re denotes the Reynolds number. Next, define $\Psi = \frac{C_{D.par}}{C_f}$, which is the ratio of a flapping wing's parasitic drag coefficient to a flat sheet's frictional drag coefficient. For most birds, this coefficient (Ψ) is moving from 2 to 4.4 [11]. For ESB-I Ψ is chosen as 4.4. The parasite drag is then determined using and the drag coefficient for a wet sheet, which is obtained as follows:

$$D_{par} = C_{D,par}\frac{\rho}{2}U_{gl}^2 S_{wet} = \Psi C_f \frac{\rho}{2}U_{gl}^2(2S) \tag{32}$$

Where S_{wet} is the sum of the wings' wet surfaces, and taken as $S_{wet} = 2S$. Then using the lift-weight relation the total Drag force can be given as:

$$D_g = \Psi C_f \frac{\rho}{2}U_{gl}^2(2S) + \frac{2K(mg\cos(\theta_{gl}))^2}{\pi AR\rho S U_{gl}^2} \tag{33}$$

Thus inserting expression of total drag during gliding phase in to (29) results:

$$P_{aero,gl} = \Psi C_f \rho U_{gl}^3 S + \frac{2K(mg)^2}{\pi AR\rho S U_{gl}} \tag{34}$$

In analog way as gliding, required aerodynamic power due to the drag in the flapping phase can be derived as follow:

$$P_{aero,fl} = D_{fl}U_{fl} \tag{35}$$

The total drag during flapping is modeled in preliminary section and it is not same as the gliding phase. A plot showing variation of different components of power during gliding and flapping phase with forward velocity is shown in Fig. 20 below.

As shown in Fig. 20 the required power for the two flight modes are not equal. While the parasite power which is due to parasite drag is the same for both flight modes, the induced power which is due to induced drag is not the same for the two flight modes.

Thus it is the induced drag component that causes the difference; while the parasite drag is the same for both flight modes, since it is not related to wing flapping but due to the form and friction of the wing and body of FWMAV.

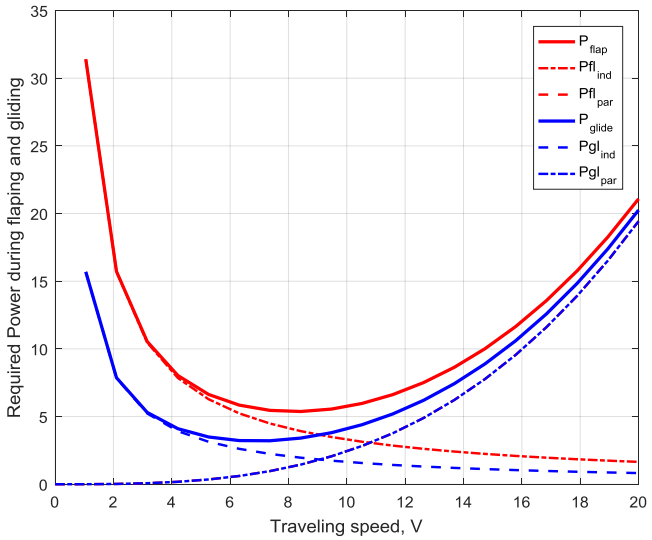

Fig. 20. Variation of power with forward velocity during gliding and flapping phase

During flapping, there are two mechanisms that create an increase in induced drag. (1) In the course of flapping, changes in the direction of the lift vectors at the left and right wings. Because of lift vector tilting, more lift must be created in flapping flight than is required for vertical force balancing. The resultant drag increases when the lift is increased. (2) Changes in magnitude of the lift vectors as the flapping cycle progresses. Including these flapping effects in the induced drag factor (i.e. $K_{flap} = aK$, a is constant consisting effects of wing flapping motion), the total drag during flapping expressed as:

$$D_{fl} = \Psi C_f \frac{\rho}{2} U_{fl}^2 (2S) + \frac{2K_{flap}(mg\cos(\theta_{cl}))^2}{\pi AR\rho S U_{fl}^2} \tag{36}$$

Then aerodynamic power during flapping can be given by:

$$P_{aero,fl} = \Psi C_f \rho U_{fl}^3 S + \frac{K_{flap}}{\pi AR} \frac{2(mg\cos(\theta_{cl}))^2}{\rho U_{fl} S} \tag{37}$$

In flap-glide flight mode, the mechanical power output available from the flapping wing mechanism in the flapping phase (P_{ava}) must be greater than the aerodynamic power in that phase ($P_{aero,fl}$).

$$P_{ex} = P_{ava} - P_{aero,fl} \tag{38}$$

3.3.2.2 ESB-I in flap-glide flight

Here based on the approach presented in the previous section performance of ESB-I in flap-glide flight mode will be studied. Also performance of ESB-I in flap-glide mode will be compared with continious flapping flight mode.

From (23) the expression for the sinking speed of the FWMAV given as:

$$V_s = \frac{P_{ex}}{W} = \frac{P_{aero,gl}}{W} \tag{39}$$

Inserting (34)(34) into (39) results:

$$V_s = \frac{\Psi C_f \rho U_{gl}^3 S}{W} + \frac{2KW}{\pi AR\rho S U_{gl}} \tag{40}$$

From the general equation of lift, $L = Wcos(\theta_{gl}) = 0.5\rho S U_{gl}^2 C_L$, the gliding speed can be given by:

$$U_{gl}{}^2 = \frac{2Wcos(\theta_{gl})}{\rho S C_L} \tag{41}$$

At small glide angles, $U_g \approx \sqrt{(2\mathrm{mg}/\rho S C_L)}$. The speed for best glide, U_{bg}, when the FWMAV is gliding with the minimum possible total drag, is the tangent to the curve described by eq. 3.1, and is given by:

$$U_{bg} = \sqrt{\frac{2mg}{\left(\rho S\sqrt{\frac{\Psi C_f \pi AR}{K}}\right)}} \tag{42}$$

Equation (42) is related to the maximum range speed (the velocity at which the energy to fly unit distance is a minimum). And the respective minimum glide number, ε_{min} which describe the minimum drag-to-lift ratio can be obtained using the above equations as:

$$\varepsilon_{min} = \left(\frac{C_D}{C_L}\right)_{min} = 2\sqrt{\Psi C_f K/(\pi AR)} \tag{43}$$

As the FWMAV glides it descends at an angle θ_{gl} to the horizontal, This angle is established by the lift-to-drag ratio ((L/D)max = 1/ε_{min} = 1/ tan θ_{gl}). Then the gliding angle can be obtained as:

$$\theta_{gl} = \tan^{-1}(\varepsilon_{min}) \tag{44}$$

Climbing angle θ_{cl} then can be obtained using the relative duration ***a*** (the duty factor or flapping ratio) of the flapping phase and gliding angle as:

$$\tan(\theta_{fl}) = -\frac{1-a}{a}\tan(\theta_{gl}) \tag{45}$$

Now using the above discussed parameters plot the work per range in (27) with the average flap-glide velocity in (28). For this analysis a MATLAB code is written based on the above mentioned expressions. The result of performance analysis for ESB-I is shown in Fig. 21 below.

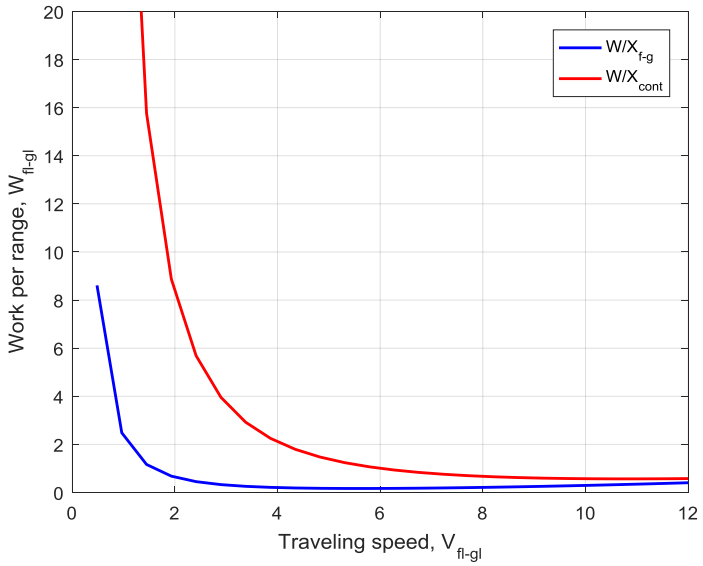

Fig. 21. Variation of Work per Range in one flap-glide cycle during flap-glide and continious flapping with flight velocity.

Fig. 21 shows comparition between flap-glide and continious flapping flight mode interms of work per Range. As can be seen there is aerodynamic advantage in flap-glide flight; The work per Range for continious flaping flight, W/X_{cont}, is higher than that of flap-glide fligh, $W/X_{f\text{-}g}$. This is because since aerodynamic cost of fixed wing is less than flapping wing (as already shown in Fig. 20), introducing gliding flight mode in to some portions of the cycle time (i.e. 1-a) will decrease the work per rang.

3.3.3 Dynamic Modeling of ESB-I

In this section dynamic modeling of ESB-I as a combination of three rigid bodies - a main body and two wings will be discussed. The main body includes fuselage and the two independent control surfaces (tails).

3.3.3.1 Reference framing

In order to determine the motion of the body in the inertial coordinate system and the position of the flapping wings, three reference frames were defined and shown in Fig. 22. These are: (1) Inertial coordinate system, *OXYZ*, with X and Y coplanar with the ground, and Z pointing up, forming an orthonormal frame; (2) the Body reference frame, ($X^BY^BZ^B$) its origin located at the center of mass (CG), with X^B aligned with the body of the FWMAV, pointing forward; Y^B axis is defined from the CG to the right wing direction and the Z^B axis forms and orthonormal frame, pointing up; (3) Wing reference frame ($X^wY^wZ^w$) is the coordinate system of the right flapping wing and its origin located at the root of the right rocker, and similar to the Body reference frame, but rotating with the wing.

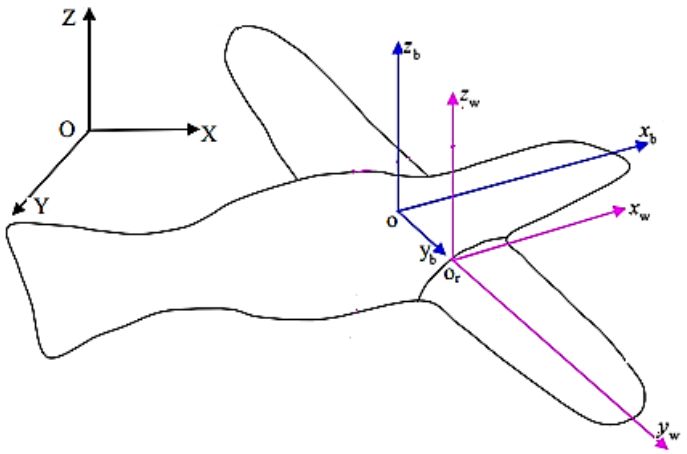

Fig. 22. Description of coordinate systems

The attitude of the FWMAV body with respect to the inertial reference frame (with the ground) will be described by the Euler roll(ϕ), pitch(θ) and yaw(ψ) angles. The orientation of the FWMAV is obtained by transforming the vector from the inertial to the body frame, using a 3-2-1 Euler angle rotation, that follows *yaw(ψ) →pitch(θ) →roll(ϕ)* order.

$$R_B^I = \begin{bmatrix} c_\theta c_\psi & c_\psi s_\theta s_\phi - c_\phi s_\psi & c_\phi c_\psi s_\theta + s_\phi s_\psi \\ c_\theta s_\psi & c_\phi c_\psi + s_\theta s_\phi s_\psi & -c_\psi s_\phi + c_\phi s_\theta s_\psi \\ -s_\theta & c_\theta s_\phi & c_\theta c_\phi \end{bmatrix} \quad (46)$$

Where $c_\theta = \cos(\theta)$, and the same for others. Then any vector described in body coordinate system V^B can be described in inertial coordinate system as: $V^I = R_B^I V^B$

As already discussed, the wings of ESB-I driven by the modified four-bar mechanism a back and forth flapping motion (plunging) will occur around the OX^B axis. Also due to the flexibility of the wing, under the action of aerodynamic as well as gravitational forces, passive pitching will occur around the OY^w axis. The attitude of the flapping wing with respect to the body therefore can be described by the flapping ($\varphi(t)$ and pitching ($\vartheta(t)$) angles respectively. The kinematic model of the wing were illustrated in preliminary stage, (1).

Since the selected flapping wing actuation mechanism gives symmetric motion for the two wings, the right and left wings, there kinematics is similar. Thus the total aerodynamic contribution of the two wings can be taken as twice the contribution of one wing.

3.3.3.2 Forces and Moments on the body

In flight process, aerodynamic forces from the two flapping wings, F_{w_aero} and tail, F_{t_aero} and gravity due to weight of the body, F_g acts normal to the FWMAV. The resultant force and moments due to the forces can be given by the equation:

$$\begin{matrix} F_t = \vec{F}_g + \vec{F}_{aero} \\ M_t = M_w + M_{tail} \end{matrix} \quad (47)$$

Where M_w and M_{tail} are wing and tail moments defined in body coordinate system respectively.

The gravitational forces of the FWMAV, $\vec{F}_g$ in body coordinate system can be given as:

$$\begin{matrix} \vec{F}_g = (R_B^I)^T [0\ 0\ mg]^T \\ = mg \begin{bmatrix} -Sin\theta \\ Cos\theta Sin\phi \\ Cos\theta Cos\phi \end{bmatrix} \end{matrix} \quad (48)$$

Where m is the mass of the FWMAV, and θ is the Pitch angle. Whereas the total aerodynamic force on the body coordinate system can be given by:

$$\vec{F}_{aero} = \vec{F}_{aero\_w} + \vec{F}_{aero\_t} \quad (49)$$

Then using (48) and (49) the total external force is given by:

$$F_t = mg \begin{bmatrix} -Sin\theta \\ Cos\theta Sin\phi \\ Cos\theta Cos\phi \end{bmatrix} + \begin{bmatrix} F_{aero,x} \\ F_{aero,y} \\ F_{aero,z} \end{bmatrix} \quad (50)$$

3.3.3.3 Flight dynamic model

The body equations of motion are developed w.r.t body-fixed axes which is assumed to be at the body center of gravity. The aerodynamic forces and moments are combined into a single term From Newton's second law, the dynamics of ESB-I can be formulated as:

$$F_t = m\frac{d}{dt} v_b + \omega_b \times m v_b \quad (51)$$

Where $\omega_b = [p\ q\ r]^T$ is the angular velocity vector of ESB-I in body coordinate system and $v_b = [u\ v\ w]^T$ is the linear velocity vector of the ESB-I in body coordinate system.

The angular equation of motion in Lagrangian form in the body axis coordinate system can be expressed by the following formula:

$$M_t = I_p \dot{\omega}_b + \omega_b \times I_p \omega_b \quad (52)$$

Where M_t is the resultant force moment of the body, I_p is the moment of inertia matrix. Then (52) can be written as:

$$\dot{\omega}_b = {I_p}^{-1}\left(M_t - \omega_b \times I_p \omega_b\right) \quad (53)$$

Now expressions for Euler angle vector, $q_{eu} = [\phi, \theta, \psi]^T$ using the transformation matrix (R_B^I) and the angular velocity (ω_b) can be obtained.

$$\omega_b = H\dot{q}_{eu} \tag{54}$$

Where H is the simplified transformation matrix between body and inertial coordinate system, R_I^B.

The angular motion equation to obtain the orientation of ESB-I relative to the inertial reference frame can be rewritten as:

$$\ddot{q}_{eu} = (I_p H)^{-1}\left(M_t - \left(H\dot{q}_{eu} \times I_p(H\dot{q}_{eu})\right) - I_p\dot{H}\dot{q}_{eu}\right) \tag{55}$$

To further simplify our angular equation, Let: $M_{hp} = I_p H$, $H\dot{q}_{eu} \times I_p H\dot{q}_{eu} = Ls$ and $C(\dot{q}_{eu}) = Ls + I_p\dot{H}\dot{q}_{eu}$, Then (55) become:

$$\ddot{q}_{eu} = {M_{hp}}^{-1}(M_t - C(\dot{q}_{eu})) \tag{56}$$

State space representation:

The general expression for nonlinear system dynamics in state space form can be given by:

$$\begin{gathered} \dot{x} = f(t, x, D) + bu(t) \\ y = h(t, x, u) \end{gathered} \tag{57}$$

Where x is system states, u is controlled input, b is adjustable parameter, y is system out put and D is total disturbance in the system (includes external disturbance and modelling uncertainty). From the system dynamic equation in (56):

$$f(t, x, D) = -\left(M_{hp}\right)^{-1} C(\dot{q}_{eu})) + D_{tot}(t) \tag{58}$$

$$bu = {M_{hp}}^{-1}(M_t)$$

$$bu = \begin{bmatrix} \frac{M_{t,x}}{i_x} + \frac{s_\theta(M_{t,z} I_y c_\phi + M_{t,y} I_z s_{\phi[t]})}{i_y i_z c_{\theta[t]}(c^2_{\phi[t]} + s^2_{\phi[t]})} \\ \frac{M_{t,y} i_z c_{\phi[t]} - M_{t,z} i_y s_{\phi[t]}}{i_y i_z (c^2_{\phi[t]} + s^2_{\phi[t]})} \\ \frac{M_{t,z} i_y c_{\phi[t]} + M_{t,y} i_z s_{\phi[t]}}{i_y i_z c_{\theta[t]}(c^2_{\phi[t]} + s^2_{\phi[t]})} \end{bmatrix} \tag{59}$$

In order to include controller action for longitudinal stability, now let's rewrite angular equation of motion of ESB-I in (56) as in the form of (57): Then dynamic equation of pitch channel considering the total disturbance in the system can be given by:

$$\begin{cases} \dot{x}_{21}(t) = x_{22}(t) \\ \dot{x}_{22}(t) = f_2\left(x_{21}(t), x_{22}(t), D_{tot}(t)\right) + b_2 u_2(t) \\ y(t) = x_{21}(t) \end{cases} \tag{60}$$

Where Pitch angle ($\theta(t)$) and its first derivative ($\dot{\theta}(t)$) are $x_{21} and\ x_{22}$ respectively, and the output y become x_{21}.

From (58) and (59) $f_2(x_{21}(t), x_{22}(t), D_t(t))$ is the second raw of $f(t, x, D)$ and $b_2 u_2$ is also the second raw of $bu(t)$. As shown in (60), the pitch channel dynamics is considered as a SISO tracking system, with the system uncertainty and external disturbance ascribed to the total disturbance, D_{tot}, which the ADRC can estimate and compensate. The roll and yaw channel dynamics can likewise be turned into a second-order SISO system using the same way; but not presented in this thesis.

In the next section based on the dynamic equation in (60), a closed loop controller, ADRC, attitude controller will be introduced to ensure longitudinal and lateral stability of ESB-I.

3.3.4 Control Surface Design for ESB-I

ESB-I adopts intermittent flapping and gliding flight which effectively combine aerodynamic advantages of fixed and flapping wings. This strategy also will give the wing movements a more natural sight, and this is essential when realizing applications of any FWMAV in surveillance. This thesis proposes active disturbance rejection controller ADRC to stabilize the attitude of ESB-I during flapping and gliding as well as the transition modes.

Even though this flight mode possesses the most significant advantages in efficiency in power consumption, however, it complicates control system design. An ADRC controller is constructed using the synergistic impacts of three components; A tracking differentiator (TD), A linear Extended State Observer (ESO) and Non-linear state error

feedback controller. These three system components solves challenges such as huge variations in system dynamics, imperfect mathematical models, and unknown external disturbances. Fig. 23 shows the block diagram of pitch channel ADRC.

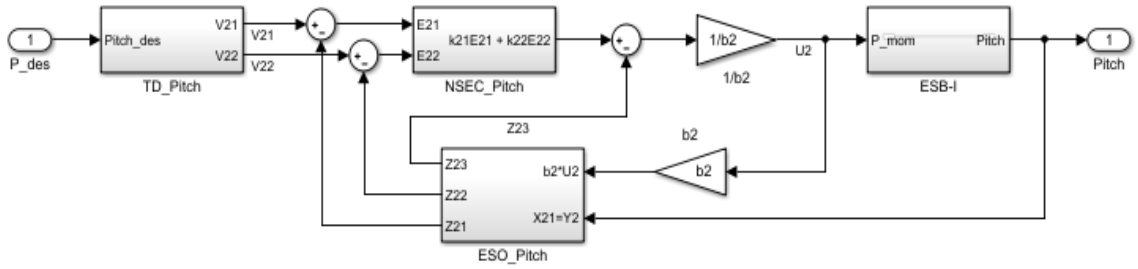

Fig. 23. General layout of ADRC

The dynamic equation for the pitch channel is already expressed in (60). Next step is designing ADRC controller for the pitch channel.

3.3.4.1 Tracking Differentiator Design

While a reference signal is transmitted it is susceptible to noise. Furthermore, the differential signal is normally generated by subtracting the reference signal backwards. TD has a good frequency filter response, but it has a noticeable limit on high-frequency oscillations. Furthermore, TD can provide a smooth and flexible process for the target tracking signal and its derivative [17]. For pitch channel it is written as:

$$\begin{cases} \dot{v}_{21}(t) = v_{22}(t) \\ \dot{v}_{22}(t) = fhan(v_{21}(t) - q_{2d}(t), v_{22}(t), r_0, h_0) \end{cases} \tag{61}$$

Here the most widely used form for tracking differentiators proposed by Han et.al in [18] is used. Where$fhan(v_{21}(t) - q_{2d}(t), v_{22}(t), r_0, h_0)$ is a nonlinear function. q_{2d} is the desired target pitch signal ($q_{2d} = \theta_d$), $v_{21}(t)$ is the tracking signal of q_{2d}, and $v_{22}(t)$ is the derivative of $v_{21}(t)$ and r_0 *and* h_0 are adjustable tracking coefficients, affecting tracking speed and smoothness. Here $v_{21}(t)$and $v_{22}(t)$are used to construct control laws. As in [18] the non-linear function is given by:

$$\begin{cases} d = r_0 h_0 \\ d_0 = h_0 d \\ y = v_{21} - q_{1d} + h_0 v_{22} \\ a_0 = \sqrt{d^2 + 8r_0|y|} \\ a = \begin{cases} v_{22} + \frac{(a_0 - d)}{2} sign(y), & |y| > d \\ v_{22} + \frac{y}{h_0}, & |y| \le d \end{cases} \\ fhan(v_{21} - q_{2d}, v_{22}, r_0, h_0) = -\begin{cases} r_0 sign(a), & |a| > d \\ r_0 \frac{a}{d}, & |a| \le d \end{cases} \end{cases} \tag{62}$$

3.3.4.2 Linear ESO Design

In this section, ESO is designed to provide the online estimation of the strongly nonlinear term, $f(x_{21}, x_{22}, D_t)$ in the dynamics of the ESB-I in addition to the state parameters. Here this term is assumed to be continuously differentiable and bounded.

To estimate a total disturbance in the system dynamic equation in (60), the unknown nonlinear function, $f(x_{21}, x_{22}, D_t)$, will be extended to a new additional system state $x_{23}(t)$. Letting $w(t) = \dot{f}(x_{21}, x_{22}, D_t)$, the system dynamics in (60) is then rewritten as:

$$\begin{cases} \dot{x}_{21} = x_{22} \\ \dot{x}_{22} = f(x_{21}, x_{22}, D_t) + b_2 u_2(t) \\ \dot{x}_{23} = w \\ y = x_{21} \end{cases} \tag{63}$$

Letting $z_{21}(t), z_{22}(t)$ *and* $z_{23}(t)$ are the estimated values of the system states x_{21}, x_{22}, and x_{23} respectively, the estimation error becomes: $e_{21} = y - z_{21} = x_{21} - z_{21}$. Then the ESO for the system defined in (63) is constructed as:

$$\begin{aligned} \dot{z}_{21} &= z_{22} + \beta_{21} e_{21} \\ \dot{z}_{22} &= z_{23} + \beta_{22} e_{21} + b_2 u_2 \\ \dot{z}_{23} &= \beta_{23} e_{21} \end{aligned} \tag{64}$$

Where $\beta_{21}, \beta_{22}\ and\ \beta_{23}$ are observer gains and according to [18] can be expressed as:

$$[\beta_{21}\ \beta_{22}\ \ \beta_{23}] = [3w_0\ 3w_0^2\ \ w_0^3] \tag{65}$$

Where w_0 is a tunable ESO bandwidth. As long as w_0 is tuned correctly, $f(x_{21}, x_{22}, D_t)$ will be approximately tracked by $x_{23}(t)$.

3.3.4.3 Nonlinear state error feedback controller design

The following are the errors between the tracking differentiator and the linear ESO:

$$\begin{cases}\varepsilon_{21} = v_{21} - z_{21} \\ \varepsilon_{22} = v_{22} - z_{22}\end{cases} \tag{66}$$

Where v_{21} and v_{22} are the target signals (given desired pitch angle and angular velocity respectively) tracked by the TD, and z_{21} and z_{22} are the observed signals of the corresponding system states. Then the nonlinear state error feedback control law for the pitch, can be given as:

$$u_2 = \frac{k_{21}\varepsilon_{21} + k_{22}\varepsilon_{22} - z_{23}}{b_2} \tag{67}$$

Where k_{21} and k_{22} are the controller parameters of the pitch channel and b_2 is an adjustable parameter.

3.4 Closed loop Simulink model

The aerodynamic, flight dynamic and controller model for our reference system, ESB-I were obtained in the previous sections. Thus the next step is to develop a SIMULINK model for the closed loop system. This model is obtained in hierarchical form with sub-systems as shown Fig. 24. These SIMULINK sub-systems will be linked together to act as a mathematical model of ESB-I. Subsequently this model will be used for longitudinal attitude control of ESB-I.

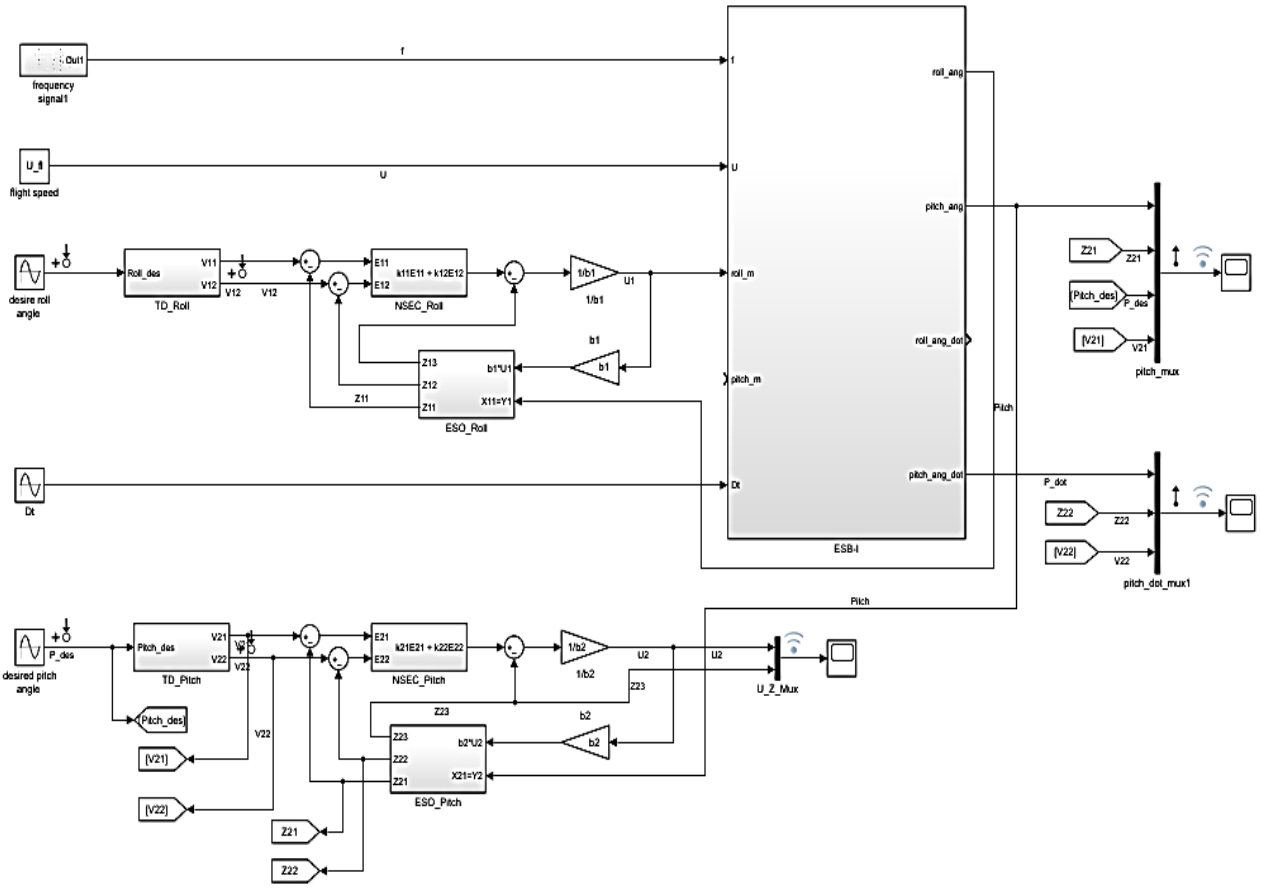

Fig. 24. Closed loop model of ESB-I

The above shows the two main blocks, namely ESB-I Block, which consists Aerodynamics and Flight dynamics subsystem blocks and the ADRC components TD, ESO and NLEFC subsystem blocks. The overall model of our reference system consists of Aerodynamic and flight dynamic model as shown in below. The aerodynamic model was obtained using MATAB files from preliminary stage with some modification. While the flight dynamic model was obtained based on the system dynamic equation.

Note that the wing section details needed for building the aerodynamics model, like wing span, area and chord length of each section, are available in the aerodynamic analysis of preliminary stage.

4. Results and Discussion

In this section, the simulations are conducted to verify the closed loop longitudinal attitude control results of ESB-I in MATLAB-Simulink platform. The required parameters in the simulations are taken from the aerodynamic analysis in the previous sections.

As already stated in the previous sections the time of flapping and gliding will be determined based on the flapping ratio and flap-glide cycle. Thus based on this in the subsequent simulations: generally the simulation takes 50s; at the beginning of the simulation from 0s to 20s, the flapping frequency is approximately 6 Hz, corresponds to flapping mode. Between 20s and 30s, then the flapping frequency reduces to 0Hz linearly, which corresponds to transition mode. Following the FWMAV will be in gliding mode. The desired pitch signal used in the simulation process is determined in the previous sections. The simulation results for the pitch angle and rate control is given in Fig. 25 to Fig. 28.

Fig. 25 shows the simulation results of pitch angle control by pitch ADRC. Where: the variable *Pitch* is the actual value of pitch angle, Z21 is ESOs estimation of Pitch, P_des is the desired pitch angle, and V21 is TDs tracking of P_des. As shown in Fig. 25, during the flapping phase (0s to 20s) even though there is a fluctuation around the desired pitch angle due to the flapping of the wings, the actual pitch angle, Pitch, tracks the desired value well. During the transition from flapping to gliding (20s to 30s) even though the linear decrease in flapping frequency causes a variation in the system dynamic, the overall tracking result is still within an acceptable range. The ADRC controller also ensures that the output pitch angle tracks the desired value well during the gliding phase; with a tracking error of less than 0.05rad. These all shows that the closed loop system with ADRC controller can effectively tracking the desired signal throughout all of the flight modes.

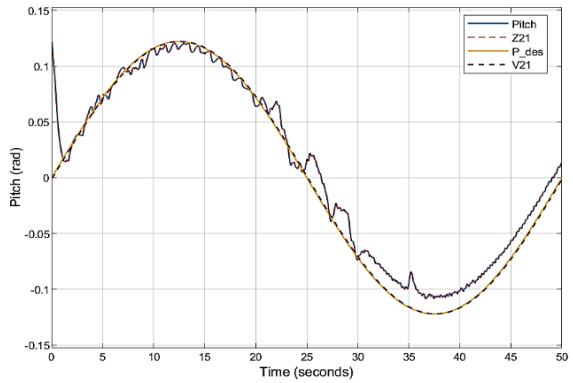

Fig. 25. Simulation result for pitch angle control under the action of Pitch ADRC.

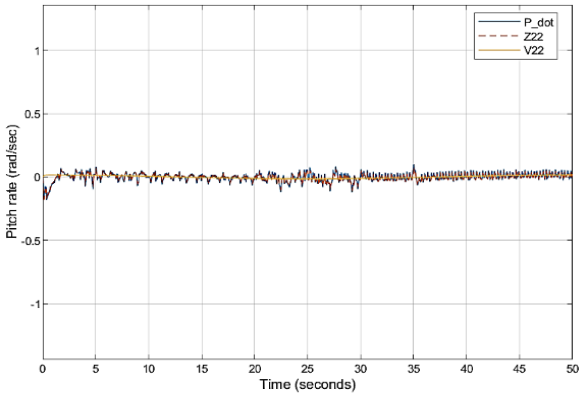

Fig. 26. Simulation result of pitch rate control under the action of pitch ADRC.

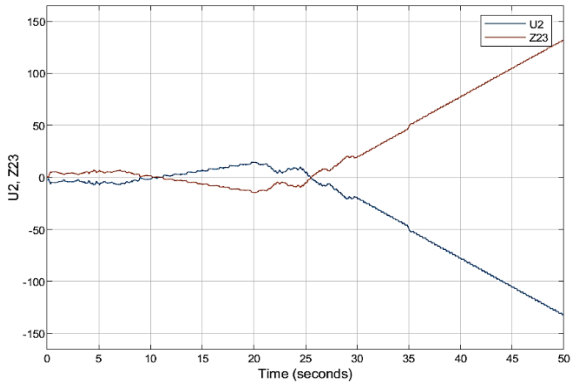

Fig. 27. Pitch channel controller output and nonlinear observation results.

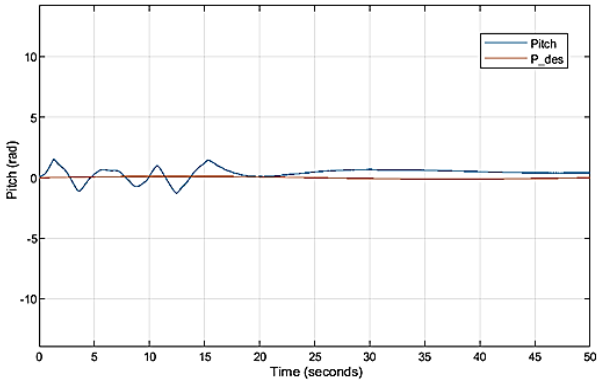

Fig. 28. Simulation result of pitch angle for the control effect of PID controller.

Fig. 26 shows the simulation results of pitch rate by pitch ADRC. Where: the variable P_dot is the actual value of pitch angle rate, Z22 is ESOs estimation of P_dot, and V22 is TDs tracking of the first derivative of the desired pitch angle, P_des. As shown in Fig. 26 even though there is a fluctuation of pitch rate around the desired one the ADRC ensures the tracking of the desired signal throughout the flight modes with a tracking error of less than 0.4 rad/sec.

Fig. 27 shows the simulation results of controller output and ESOs nonlinear observation results. Where: the variable U2 is the Pitch ADRC output and, Z23 is ESOs estimation of the nonlinear function in the system dynamics. As shown in Fig. 27 ESO can provide online estimation of the system nonlinearity throughout the flight modes and causes the controller to take action. Based on ESO- estimation the controller changes its value opposite to the system nonlinearity so that it can compensate it.

In general, all of the simulation results illustrated above shows that the closed loop longitudinal attitude stability of ESB-I can be ensured by the control effect of ADRC controller in all three flight modes. To further explain the characteristics of the ADRC, a closed loop simulation result of the pitch channel under the action of PID controller is provided and compared with ADRC simulation result.

Fig. 28 shows the simulation results of pitch angle control by the action of PID controller. Where: the variable Pitch is the actual value of pitch angle, and P_des is the desired pitch angle. Various variables values used in the simulation processes of PID controller is the same as ADRC. As shown in Fig. 28 the output of the closed loop loop pitch control system tracks the desired signal with a tracking error of greater than 1rad. This shows that throughout the three modes the tracking effectiveness of actual pitch angle under the action of PID controller is decreased by a significant level compared to action of ADRC. This outcome is because of lack of PID controller to track system dynamic variation in real time. In the contrary ADRC can track the system dynamic variation with ESO, so that it gives a better result for attitude control of FWMAV which adapt a multiple flight mode like flap-glide flight mode.

5. Conclusions and Recommendations

The research will be summarized, as well as the findings and conclusions, in this last chapter. Finally, future works are listed.

5.1 Summary of research

This thesis presented dynamic design and attitude control of a FWMAV which adapts intermittent flap-glide flight mode.

Through the first part of this thesis, a new reference model named ESB-I which adapts intermittent flap-glide flight mode was conceptually designed. In this part some achievements have been made in the design of aerodynamically efficient flapping wing and in the design of driving mechanism for ESB-I.

In the conceptual design stage, initial aerodynamic and geometric parameters of our reference model was selected using scaling law. In the next design step, preliminary stage, efficient airfoil based on the mission requirement was selected. This was done by first selecting a list of airfoils which best suited for low Reynold number ($10^4 - 10^5$) flight. Then by comparing their efficiency and performance parameters using XFLRv5 software and MATLB program, the best airfoil was chosen. After selecting airfoil aerodynamic model of ESB-I which includes unsteady effects was developed.

The detail actuation mechanism design process was completed after the sizing procedure and aerodynamic study that resulted to the identification of geometric and aerodynamic parameters of ESB-I. The developed mechanism is a hybrid of the alternating four bar configuration and the slider crank mechanism, combining the benefits of both types of actuation methods while avoiding their disadvantages. The extreme symmetry of this mechanism, as well as all of its hinged connections, are two of its most notable aspects.

The ESB-I's performance in flap-glide flap mode was investigated. Because the aerodynamic cost of a flapping wing is higher than that of a fixed wing, the possibility of a gliding flight phase, such as that found in flap-gliding flight, yields a performance advantage over continuous flapping flight due to the lower aerodynamic cost. When mathematical relations describing flap-gliding flight in terms of work per range of one flap-glide cycle are presented, it is proven that flap-gliding flight saves energy over continuous flapping flight over. In the lower speed range, the energy savings are at their peak.

After successfully designing our reference model, ESB-I, dynamic modeling of the system was followed. This model combines the unsteady aerodynamics effects of the flapping wing model based on modified strip theory approach and multi-body flight dynamics model. The overall body was considered as three rigid body with the two wings and the fuselage which includes the tail. Since the selected flapping wing actuation mechanism gives symmetric motion for the two wings while modeling the two wings, their kinematic and dynamic contributions were taken as similar. Thus taking aerodynamic contributions of the wings and tail and the weight of body as external forces, flight dynamic of ESB-I was successfully modelled in MATLAB/SIMULINK platform. The dynamic model was built in the way that it can be used to identify the position and orientation of the system with respect to the ground.

Adapting the flap-glide flight mode has substantial advantages in terms of efficiency in power consumption, but it presents challenges in control system design, particularly during transitions between flapping and gliding. An ADRC controller was successfully constructed for the longitudinal attitude stabilization of ESB-I operating in flap-glide flight mode to address concerns connected to substantial fluctuations in system dynamics.

Lastly this thesis provides simulation results of the closed loop system. It is shown that introducing ADRC into the system guaranties the attitude stability of ESB-I. Comparison of the closed loop system response with PID controller and ADRC was also studied. It is prove that ADRC give stunning response than PID controller.

5.2 Future work and Recommendation

Computational tasks could be completed to improve the aerodynamic, flight dynamic and control system modeling results and provide more insight into FWMAV flight. These tasks are summarized below:

1. Through consecutive computational tasks overall system of ESB-I can be developed to achieve high aerodynamic efficiency and performance. This can be done by using novel sizing method for sizing the wings, tail and fuselage, by selecting appropriate electrical and structural equipment's for the designed platform based on aerodynamic and performance requirement
2. Improving aerodynamic model of ESB-I by including other unsteady aerodynamic effects that were not included in this thesis, by considering aero elastic effect on the aerodynamic model. The aerodynamic model of the tail can also be improved to include a more extended flight envelope.
3. Improving dynamic model of ESB-I by including actuator dynamics
4. Extending the control architecture to include lateral and directional attitude control, as well as altitude and flight speed control.
5. Analyzing Application for ESB-I

References

[1] B. J. Goodheart, "Tracing the History of the Ornithopter: Past, Present, and Future.," Journal of Aviation/Aerospace Education and Research, vol. 21, no. 1, 2011.

[2] M. Malik and F. Ahmad, "Effect of Different Design Parameters On Lift, Thrust and Drag of an Ornithopter," Proceedings of the World Congress on Engineering, vol. II, 2010.

[3] W. Shyy, M. Berg and D. Ljungqvist, "Flapping and flexible wings for biological and micro air vehicles," Progress in Aerospace Sciences, vol. 35, pp. 455-505, 1999.

[4] G. L. Gao, "Research on dynamic model and flight simulation for micro air vehicles.," 2011.

[5] W. Yang, L. Wang and B. Song, "Dove: A biomimetic flapping-wing," International Journal of Micro Air Vehicles, vol. 0, pp. 1-15.
[6] M. Hassanalian and A. Abdelkefi, "Towards Improved Hybrid Actuation Mechanisms for Flapping Wing Micro Air Vehicles: Analytical and Experimental Investigations," Drones, 2019.
[7] M. Hassanalian and A. Abdelkefi, "Methodologies for weight estimation of fixed and flapping wing micro air vehicles," Meccanica, 2016.
[8] A. S. Taimur, A. S. Syed Irtiza, J. Ali and R. H. Syed Hossein, "Airfoil Selection Procedure, Wind Tunnel Experimentation and Implementation of 6DOF Modeling on a Flying Wing Micro Aerial Vehicle," Micromachinee, 2020.
[9] "airfoiltools.com," [Online].
[10] J. D. DeLaurier, "An aerodynamic model for flapping-wing flight," The Aeronautical Journal of the Royal Aeronautical Society, April 1993.
[11] R. L. Harmon, "AERODYNAMIC MODELING OF A FLAPPING MEMBRANE WING USING Motiion Tracking Experiments," 2008.
[12] R. Jones, "The unsteady lift of a wing of finite aspect ratio," NACA, 1940.
[13] J. Scherer, "Experimental and theoretical investigation of large amplitude oscillation foil propulsion systems," Hydraunautics, 1968.
[14] T. Theodorsen, "General theory of aerodynamic instability and the mechanism of flutter," NACA, 1935.
[15] I. Garrick, "Propulsion of a flapping and oscillating aerofoil.," NACA, 1936.
[16] "Flight and scaling of flyers in nature," in Flow Phenomena in Nature, Sweden, Department of Zoology, University of Göteborg, 2006, pp. 122-154.
[17] K. W. J.-N. C. X. Y. Chang-Chun Hua, "Tracking differentiator and extended state observer-based nonsingular fast terminal sliding mode attitude control for a quadrotor," 2018.
[18] J. Han, "From PID to active disturbance rejection control," IEEE Transact Industrial Electronics , pp. 900-906, 2009.
[19] Hoerner and F. S, "Skin-friction drag," Fluid dynamic drag, 1965.
[20] J. M. V. Rayner, P. W. Viscardi, W. Sally and J. R. Speakman, "Aerodynamics and Energetics of Intermittent Flight in Birds," AMER. ZOOL., vol. 41, pp. 188-204, 2001.
[21] S. Linang, B. Song and J. Xuan, Active Disturbance Rejection Attitude Control for a Bird-Like Flapping Wing Micro Air Vehicle During Automatic Landing, vol. 8, 2020.
[22] H. Djojodihardjo, "An Assessment of a Linear Aerodynamic Modeling of a Generic Flapping Wing Ornithopter," International journals of Astronoutics and Aeronoutical Engineering, 2018.
[23] H. Liu, T. Nakata, N. Gao, M. Maeda, H. Aono and W. Shyy, "Micro air vehicle-motivated computational biomechanics in bio-flights: aerodynamics, flight dynamics and maneuvering stability," 2010.
[24] A. Q. K. a. Rini, "Review on System Identification and Mathematical Modeling," Applied sciences, 2021.
[25] S. Liang, B. Song and J. Xuan, "Active disturbance rejection attitude control for the dove flapping wing micro air vehicle in intermittent flapping and gliding flight," 2020.
[26] C.-C. Hua, K. Wang, J.-N. Chen and X. You, "Tracking differentiator and extended state observer-based nonsingular fast terminal sliding mode attitude control for a quadrotor," 2018.
[27] Huang and Mingyang, "Optimization of flapping wing mechanism," Journal of Aerospace Engineering, 2018.
[28] B. B. R. S., M. A. A. Nugroho, Y. S. A., B. R. Trilaksono and A. Moelyadi, "Dynamic Modeling using System Identification and Attitude Control Design of GaneFly Flapping Wings Micro Aerial Vehicle (FWMAV)," in 7th IEEE International Conference on System Engineering and Technology, 2017.
[29] P. Chirarattananon, Y. Chen, E. F. Helbling, K. Y. Ma and R. C. a. R. J. Wood, "Dynamics and flight control of a flapping wing robotic insect in the presence of wind gusts," Interface Focus, 2016.
[30] A. A. Paranjape, M. R. Dorothy and S.-J. C. a. K. D. Lee, "A Flight Mechanics-Centric Review of Bird-Scale Flapping Flight," International Journals of Aerooutic and Space Sciences, 2012.

Author's Profile

Lidiya Abebe Dejene received Bsc and Msc degree in Mechatronic Engineering from Hawassa University, Hawassa and Addis Ababa Science and Technology University Addis Ababa Ethiopia, in 2016, 2022 respectively.

She is currently a lecturer in Wachemo University, Ethiopia. Her research interest includes control of flapping wing micro air vehicles, Nano air vehicles, space vehicles.

How to cite this paper: Lidiya Abebe Dejene, "Dynamic Modelling and Control of Flapping Wing Micro Air Vehicle for Flap-Glide Flight Mode", International Journal of Engineering and Manufacturing (IJEM), Vol.12, No.5, pp. 22-47, 2022. DOI:10.5815/ijem.2022.05.03